Proc. Natl. Acad. Sci. USA
Vol. 92, pp. 11721–11725, December 1995
Biochemistry

Crystal structure of the complex of a catalytic antibody Fab fragment with a transition state analog: Structural similarities in esterase-like catalytic antibodies

(phosphonate hapten/ester hydrolysis/oxyanion hole/hapten-induced conformational change)

JEAN-BAPTISTE CHARBONNIER*, ELIZABETH CARPENTER*†, BENOÎT GIGANT*, BÉATRICE GOLINELLI-PIMPANEAU*, ZELIG ESHHAR‡, BERNARD S. GREEN§, AND MARCEL KNOSSOW*¶

*Laboratoire de Biologie Structurale, UMR 9920, Centre National de la Recherche Scientifique, Université Paris Sud, Bât. 34, Avenue de la Terrasse, 91198 Gif-sur-Yvette Cedex, France; ‡Department of Chemical Immunology, Weizmann Institute, Rehovot, Israel; and §Department of Pharmaceutical Chemistry, The Hebrew University School of Pharmacy, Jerusalem 91120, Israel

Communicated by Don C. Wiley, Harvard University, Cambridge, MA, July 24, 1995

ABSTRACT **The x-ray structure of the complex of a catalytic antibody Fab fragment with a phosphonate transition-state analog has been determined. The antibody (CNJ206) catalyzes the hydrolysis of *p*-nitrophenyl esters with significant rate enhancement and substrate specificity. Comparison of this structure with that of the uncomplexed Fab fragment suggests hapten-induced conformational changes: the shape of the combining site changes from a shallow groove in the uncomplexed Fab to a deep pocket where the hapten is buried. Three hydrogen-bond donors appear to stabilize the charged phosphonate group of the hapten: two NH groups of the heavy (H) chain complementarity-determining region 3 (H3 CDR) polypeptide chain and the side-chain of histidine-H35 in the H chain (His-H35) in the H1 CDR. The combining site shows striking structural similarities to that of antibody 17E8, which also has esterase activity. Both catalytic antibody ("abzyme") structures suggest that oxyanion stabilization plays a significant role in their rate acceleration. Additional catalytic groups that improve efficiency are not necessarily induced by the eliciting hapten; these groups may occur because of the variability in the combining sites of different monoclonal antibodies that bind to the same hapten.**

The exquisite stereospecificity and high turnover number of enzymes make them high-profile targets for bioorganic chemists, who aim both to understand and mimic these catalysts. Enzyme catalysis is understood to occur because enzymes selectively bind the transition state for a step of a particular reaction (1, 2). To create binding entities with a catalytic potential, synthetic host molecules have been made (3), and enzymes have been altered to change their specificity without destroying their catalytic activity (4, 5). Another approach has been to use the remarkable capacity of the immune system, which generates antibodies possessing high binding affinity and structural specificity towards virtually any molecule, to produce catalytic antibodies ("abzymes") (6).

The majority of known catalytic antibodies have been programmed to catalyze the hydrolysis of esters as well as other acyl transfer reactions. They have been raised against phosphonate haptens, transition state analogs (TSA) that model the structure of the putative tetrahedral transition states of these reactions. The catalytic activity exhibited by these antibodies is generally far below that of enzymes. The catalytic proficiency of these antibodies can be improved with phage display libraries (7) and development of effective screening methodologies (8, 9). For all monoclonal catalytic antibody approaches, it is important to understand the relationship between the TSA and the structure of the catalytic antibody raised against it (10). To this end, we have determined the structure of the Fab fragment of an esterase-like catalytic antibody, CNJ206, with bound hapten; the conformation of the combining site differs from the one previously found in uncomplexed CNJ206 (11).

Antibody CNJ206 catalyzes the hydrolysis of *p*-nitrophenyl ester (compound **1** in Fig. 1) with significant rate enhancement (k_{cat}/k_{uncat} = 1600) and substrate specificity and displays multiple cycles (12). CNJ206 has been obtained by immunization with a keyhole limpet hemocyanin conjugate of phosphonate hapten **2** in Fig. 1 and has been selected for its high affinity for the short TSA **3** in Fig. 1 (13). We report here the structure of CNJ206 Fab fragment complexed with **3**.‖ We describe the amino acids present in the combining site, analyze their relationship with the inducing hapten, and discuss their possible role in catalysis; we then compare this structure to that of Fab 17E8, the only other catalytic antibody Fab with esterase activity whose structure has been solved (14).

MATERIALS AND METHODS

Affinity and Kinetic Measurements. K_m and k_{cat} for hydrolysis of **1** were determined as described (13). Affinity measurements were performed on the CNJ206 Fab by an indirect ELISA procedure (15).

Crystallization and Data Collection. The preparation of monoclonal antibody CNJ206, hapten **3**, and the preparation and purification of CNJ206 Fab have been reported (11). The hanging drop procedure was used to grow crystals by vapor diffusion; they were obtained in drops consisting of 2 μl of the protein solution and 2 μl of a precipitating solution [8% (wt/vol) polyethylene glycol 10,000/17% (vol/vol) glycerol/0.5 mM $ZnSO_4$/1 mM hapten **3** in 0.1 M Tris·HCl, pH 8.0/0.05% NaN_3]. The initial protein solution was concentrated at 10 mg/ml; the drop was equilibrated against a reservoir solution that consisted of the precipitating solution without TSA and to which 0.15 M NaCl was added.

Intensity data were collected on one crystal kept at 4°C on the W32 station of the Laboratoire pour l'Utilisation du Rayonnement Electromagnetique (Orsay, France) synchrotron using a MAR Image Plate system. The crystal belongs to symmetry

The publication costs of this article were defrayed in part by page charge payment. This article must therefore be hereby marked "*advertisement*" in accordance with 18 U.S.C. §1734 solely to indicate this fact.

Abbreviations: H and L chains, heavy and light chains; C, constant; V, variable; TSA, transition-state analog; CDR, complementarity-determining region; H1–H3 CDR, H chain CDRs 1–3.

†Present address: National Institute for Medical Research, The Ridgeway, Mill Hill, London NW7 1AA, United Kingdom.
¶To whom reprint requests should be addressed.

‖The atomic coordinates have been deposited in the Protein Data Bank, Chemistry Department, Brookhaven National Laboratory, Upton, NY 11973 (reference IKNO).

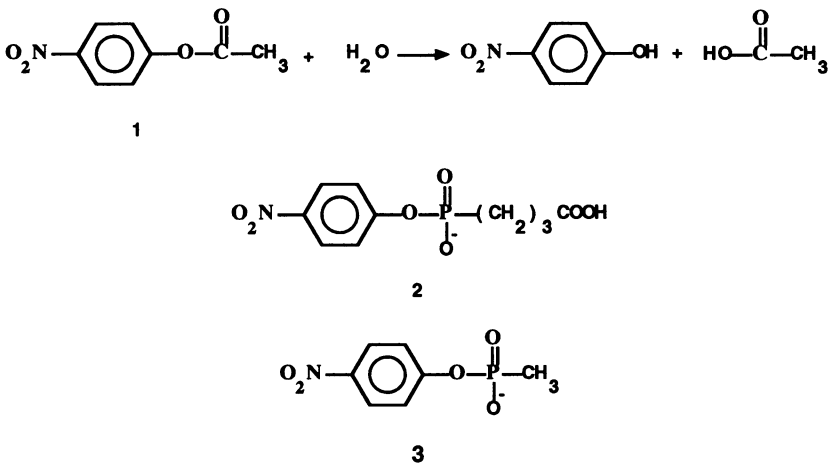

1

2

3

FIG. 1. Diagrams of the hydrolysis catalyzed by antibody CNJ206 and of the compounds used in this study. **1** is the substrate (*p*-nitrophenyl acetate); **2** and **3** are different analogs used in this study: **2** is the TSA hapten used to elicit CNJ206, and **3** is a short TSA used to select this catalytic antibody. The structure presented here is the complex between CNJ206 and **3**.

of space group *P*1 with a = 74.1 Å, b = 76.9 Å, c = 88.3 Å, α = 93.8°, β = 93.9°, and γ = 115.6°. Intensities were evaluated with the program MOSFLM as modified for the image plate (16) and were processed with programs of the CCP4 suite (17), giving an overall R_{merge} of 11.2%. The data set used for structure analysis had 27,401 unique reflections in the 20- to 3.2-Å resolution range with 96% completion (89% in the 3.3- to 3.2-Å shell; 41% of the reflections in that shell were larger than 2 SD; R_{merge} in that shell was 44%). These data were measured with a 1.8 redundancy.

Structure Determination. The structure was solved by molecular replacement with the program AMoRe (18) and data in the 10- to 4-Å resolution range. The Fv and the constant (C) domain C_L–C_{H1} dimer of the unliganded CNJ206 Fab (11) were used separately as models for the corresponding parts of the complex. At the end of molecular replacement, the model consisting of three Fvs and three C domain dimers had an R factor of 0.32 for data in the 10- to 4-Å range. The three Fabs in the asymmetric unit are related by two pseudo-twofold symmetry operations.

The model was refined by using the conjugate-gradient protocol in X-PLOR (19), and progress was judged by decrease of the free R factor (20). Noncrystallographic symmetry restraints were applied to the framework regions of the Fv and C_L–C_{H1} domains separately. Complementarity-determining regions (CDRs) were checked and rebuilt in omit difference maps with the O program (21). Electron density for the hapten was clearly visible in the combining site on F_o-F_c maps; we could distinguish the phosphonate from the *p*-nitro substituent of the hapten because it is the only feature in the map where the F_o-F_c difference map is >9.0 SD, the next highest peak being at a height of 5.5 SD. The final R factor is 20% for all data larger than 2 SD in the 7- to 3.2-Å resolution range used in refinement (R_{free}: 27.2%), with a standard stereochemistry as evaluated with PROCHECK (22). No water molecule was included in the refinement. The method of Luzzati (23) gives an estimate of 0.35 Å for the overall mean position error from the variation of the R factor with the resolution. Coordinates have been deposited with the Protein Data Bank (24).‖ Residue numbering used here is sequential and differs from that in the published CNJ206 sequence (12).

Analysis of the Model. Superposition of atomic models was done with program SUPERPK (P. Alzari, personal communication), which implements the algorithm of Kabsch (25). Coordinates for 17E8 and unliganded CNJ206 Fabs were obtained from the Protein Data Bank (24) (data set codes: 1EAP and 2GFB, respectively). Surfaces were calculated by using the algorithm of Shrake and Rupley (26).

RESULTS

Association Constants for Species Along the Path of the Reaction Catalyzed by CNJ206. K_m and k_{cat} for the hydrolysis of compound **1** in Fig. 1 (K_m = 80 ± 10 μM; k_{cat} = 0.4 ± 0.05 min^{-1}) are very similar to values obtained previously with the Fab and the *p*-nitrophenyl ester of *N*-glutaryl caproate (11, 12); they were measured at the pH (pH 8) of the crystal growth. K_d for the *p*-nitrophenol product was measured at this pH and at pH 4, well below the pK of *p*-nitrophenol (pK = 7.15). The dissociation constant for *p*-nitrophenol at pH 4 (K_d = 30 ± 3 μM) is much lower than at pH 8 (K_d > 3 mM).

Conformational Changes in the Fab upon Hapten Binding. The structure of the uncomplexed CNJ206 Fab has been solved at 3.0-Å resolution and reported (11). The conformation of the C domain dimer is essentially unchanged in the complex and uncomplexed structures (rms deviation of C^α positions: 0.4 Å; 190 atoms compared), but there is a significant rearrangement of the Fv (rms deviation of C^α positions: 1.0 Å; 208 atoms compared). Since individual light (L) and heavy (H) chain variable (V) domains V_L and V_H [except the CDR3 of the H chain (H3 CDR)] superimpose very well to the corresponding domain in uncomplexed CNJ206 (rms deviation of C^α positions 0.36 Å and 0.49 Å, respectively; 105 atoms compared), the observed rearrangement is due to a movement of one of the V domains with respect to the other. This movement can be decomposed into a rotation (7°) followed by a 0.9-Å translation parallel to the rotation axis. Such structural changes have been previously observed in several Fabs upon hapten or antigen binding (27).

In addition to the rearrangement of the Fv fragment's two domains, there is a significant change of the H3 CDR [H chain arginine-98 (Arg-H98) to Tyr-H108] conformation in the complexed CNJ206 structure (Fig. 2). In particular, in the uncomplexed CNJ206 structure, Tyr-H101 prevents the formation of the deep pocket usually observed in the combining site of antibodies specific for small molecule haptens (29); in the CNJ206·**3** complex, the plane of the phenyl ring of Tyr-H101 is approximately at a right angle to its orientation in unliganded CNJ206. This enlarges the cavity, where the hapten is found, towards the external medium. Mainly as a result of the H3 CDR movement, the shape of the combining site in unliganded CNJ206 changes from a shallow groove to a deep pocket in CNJ206·**3**.

Interaction of the Hapten with the Active Site. The TSA buries 95% of its accessible surface (345 $Å^2$ out of 360 $Å^2$) in the complex in a cavity mainly delimited by the L and H chains of CDR3; both CDR3 chains together contribute 41% to the buried surface of the hapten. The rest is due mostly to framework residues and to the other CDRs. Compound **3** is oriented so that the phosphonate is closest to the outside of the antibody, whereas the hydrophobic *p*-nitrophenyl group is buried deep inside the cavity. This orientation is consistent with the phosphonate being closest to the attachment site of the inducing hapten **2** to the carrier protein.

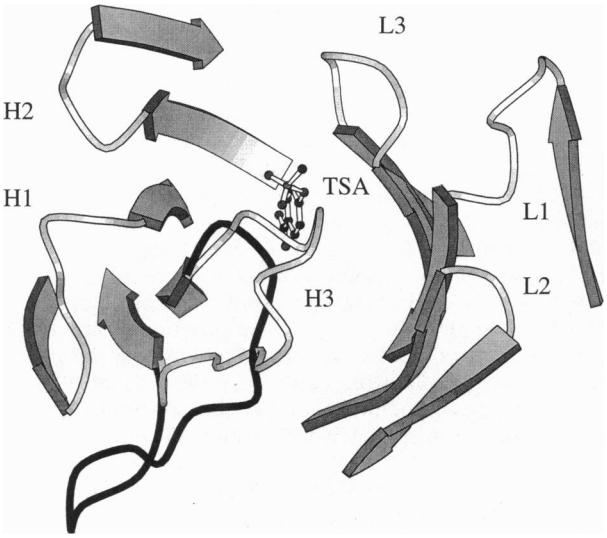

FIG. 2. Rearrangement of the CNJ206 Fab combining site upon hapten **3** binding. A ribbon diagram of the overall structure of the complex is shown. The hapten is drawn in ball-and-stick representation. The light chain (L) and the heavy chain (H) of CNJ206 Fab are respectively on the right- and on the left-hand side. The conformation of the H3 CDR observed in the uncomplexed CNJ206 structure is shown in black. A large movement of the H3 loop is observed upon hapten binding, which results in a higher complementarity between the combining site and the hapten. Figs. 2, 5, and 6 were made with MOLSCRIPT (28).

We will now describe the details of the combining site cavity and compare it with that of 17E8 (14). The cavity contains a large proportion of aromatic residues and the *p*-nitro group of **3** is in a very hydrophobic environment at the bottom of the combining site pocket (Fig. 3 *Upper*). The phenyl ring of the TSA is surrounded by the phenyl rings of two tyrosine residues (Tyr-L96 and -H101) and by the imidazole of His-H35. The bottom of the cavity is made by the same residues as in 17E8 (Fig. 3 *Lower*). As one goes towards the external medium, from the nitro group to the phenyl group of **3**, the cavities in 17E8 and CNJ206 become more different. In the superposition of the two antibody–TSA complexes, the phenyl ring of **3** overlaps with the hapten phosphonate in 17E8; the latter group is surrounded by Arg-L96 (Tyr-I96 in CNJ206), Lys-H97 (Ala-H97 in CNJ206), and His-H35 (the same in CNJ206).

The phosphonate part of **3** makes contacts with the H3 CDR at the entrance of the combining site pocket. The location of the phosphorus and phenolic oxygen atoms are unambiguously defined (Fig. 4). Given the moderate resolution of the data, the rotamer of the phosphonate part of **3** is not defined by the electron density. Three hydrogen bond donors that potentially stabilize the negatively charged phosphonate are identified on the basis of distance criteria; two of them are unambiguous—the peptide NH groups of two consecutive residues of the H3 CDR (Fig. 5). The third hydrogen bond donor is the $N^{\varepsilon 2}$ of His-H35. In Fab H chains, the H35 residue makes a conserved hydrogen bond with Trp-H47 (31). Histidine residues can have two rotamers that cannot be distinguished in electron-density maps. We have chosen the His-H35 rotamer of the present model so that the conserved hydrogen bond between this residue and the indole NH of Trp-H47 can be made; this brings the $N^{\varepsilon 2}$ hydrogen within bonding distance of the phosphonate of **3.** The presence of three hydrogen bond donors in the immediate neighborhood of the two partially charged phosphonate oxygens strongly suggests that hydrogen bonds between these atoms stabilize the TSA when bound to CNJ206. The assignment of the hydrogen bonds made between the three hydrogen bond donors we have identified and the two partially charged oxygen atoms of the phosphonate in **3** depends on the orientation chosen for this group and should be considered as tentative. In the orientation we present, the two oxygens of the phosphonate make three hydrogen bonds with atoms of CNJ206 (Fig. 5).

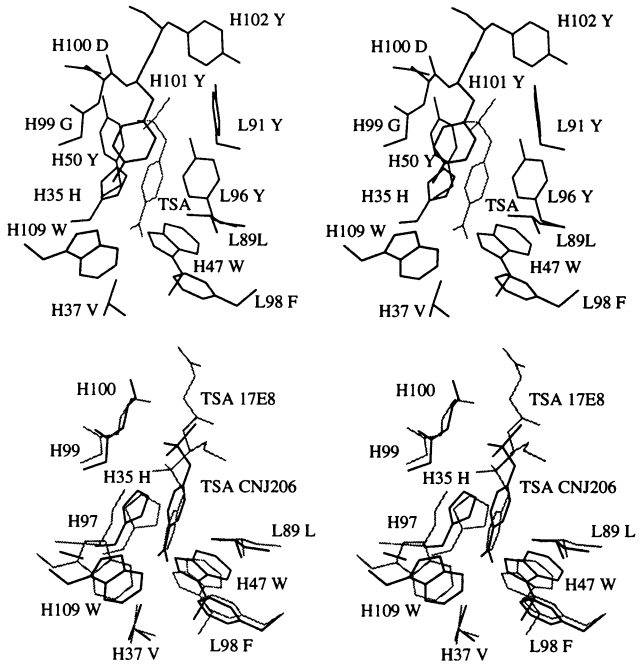

FIG. 3. (*Upper*) Stereoview of the CNJ206 binding site. The TSA is shown in light grey. The TSA environment is shown in dark grey. The *p*-nitro group binding pocket is composed of the hydrophobic side chains of Val-H37, Trp-H47, Trp-H109, Leu-L89, and Phe-L98. The phenyl ring of the short TSA contacts the phenyl rings of Tyr-L96 and Tyr-H101 and the imidazole of His-H35. The phosphonate group at the entrance of the combining site pocket makes hydrogen bonds with the H3 CDR main chain (Asp-H100 and Tyr-H101 NH groups) and with His-H35. (*Lower*) Superposition of the combining sites of CNJ206 and 17E8. 17E8 residues are in light grey, CNJ206 residues are in dark grey, and all are numbered as in CNJ206. The phenyl group of the phenyl norleucine phosphonate TSA of 17E8 overlaps with the nitro group of the TSA in CNJ206. Figs. 3 and 4 were made with the O program (21).

DISCUSSION

Catalytic Mechanism. The base-catalyzed hydrolysis of esters proceeds through the formation of negatively charged tetrahedral transition states; their stabilization would decrease the activation energy barrier and therefore increase the reac-

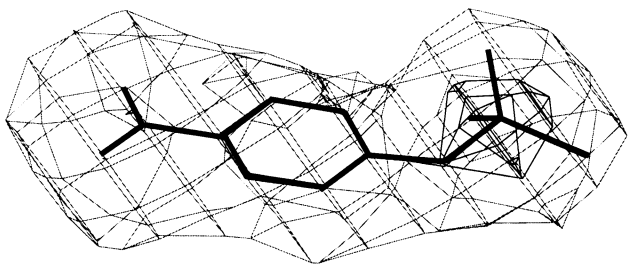

FIG. 4. Averaged $2F_o-F_c$ electron density in the combining site. This map was obtained using the program AVERAGE (30); it is contoured at 1 and 8 SD levels (respectively light and dark lines). The latter contour unambiguously defines the position of the phosphorus atom. The electron density around the phosphonate is spherical and does not allow one to define the orientation of the methyl group and the two negatively charged oxygens only from the electron density.

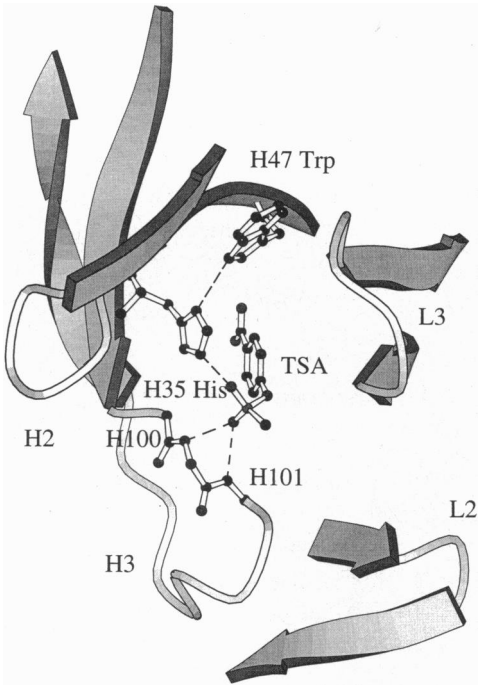

FIG. 5. Hydrogen bonds in the combining site involved in the stabilization of TSA **3**. The interactions between the two partially negatively charged oxygens of the phosphonate and the combining site are formed by the peptide NH from two consecutive residues in the H3 CDR (distances 2.6 Å and 2.7 Å) and by $N^{\varepsilon 2}$ of His-H35 (distance 2.9 Å). The potential hydrogen bond shown between the indole NH of residue Trp-H47 and residue H35 (a histidine in CNJ206) is a structurally conserved feature of Fabs.

tion rate. CNJ206 selectively stabilizes the transition state structure, as reflected in the higher affinity for hapten **3** (K_d = 1.1 μM) as compared with substrate **1** (K_m = 80 μM). The structural differences between the TSA and substrate are localized to the negatively charged tetrahedral phosphonate group. In the CNJ206·**3** complex there are three potential hydrogen bonds to the negatively charged phosphonate, as seen in Fig. 5; these hydrogen bonds should be much stronger than those with the substrate carbonyl oxygen, which is neutral (32). This correlates with the higher affinity for **3** than **1**.

Ester hydrolysis transition states present a single negative charge on the oxyanion. According to our structure, the hydrogen bonds stabilizing this oxyanion can be either with the peptide NH of two consecutive residues in the H3 CDR or with the $N^{\varepsilon 2}$ of His-H35. The former possibility differs from the arrangement found in the trypsin family of serine proteases, where the oxyanion hole is made of two peptide NH bonds; in these enzymes the NH groups involved belong to residues n and $n+2$ (193 and 195 with the numbering of chymotrypsin). In subtilisin, oxyanion stabilization has been found to provide an acceleration of the same order of magnitude as that observed in CNJ206 (33). Oxyanion stabilization might therefore be all that is involved in catalysis by CNJ206, but is difficult to quantitate. We discuss in the next section the additional contributions to the rate acceleration that might come from other residues of CNJ206 Fab, if oxyanion stabilization were not all that is required to account for catalysis.

Additional contribution to catalysis in CNJ206 could come from polar residues close to the phosphonate of **3**. All of these residues (His-H35, Tyr-H50, Tyr-H102 and Tyr-L96) have their polar groups further than 4.1 Å from the phosphorus of **3** (Fig. 3 *Upper*); a nucleophilic attack by one of them on the carbonyl of the ester substrate would therefore necessitate a significant rearrangement of the CNJ206 combining site during catalysis. An alternative possibility is a direct hydroxide attack at the substrate carbonyl, which may be general base-catalyzed. Assuming that substrate **1** occupies the same general position as TSA **3**, it is possible to position a water molecule relative to the carbonyl of **1** in a configuration close to the one predicted to be favorable for nucleophilic attack (34), so that it would make a hydrogen bond with His-H35 (Fig. 6); its deprotonation could then be assisted by the imidazole base of His-H35. This requires that the oxyanion hole is comprised solely of the H3 CDR peptide NH groups and assumes that the potential hydrogen bond of His-H35 with the indole NH of Trp-H47 does not permanently orient its nucleophilic nitrogen away from the combining site cavity. The structure of the CNJ206·**3** complex also suggests that additional rate acceleration could be gained by mutating Tyr-L96 (Fig. 3 *Upper*) to histidine, whose imidazole could play the role of a general base. If the present conformation of the combining site were maintained, the mutant His-L96 would not interact directly with **3**.

The last step in the catalytic cycle is product release; since the *p*-nitrophenol product structure comprises *ca.* 70% of the transition state analog **3** structure, *p*-nitrophenol might be expected to bind and lead to product inhibition. Indeed, unionized *p*-nitrophenol is bound at pH 4, but at pH 8, where catalysis has been measured, there is no measurable affinity of CNJ206 for the charged *p*-nitrophenolate. The delocalized negative charge of this product at pH 8 is expected to disfavor binding in the hydrophobic cavity found in the CNJ206·**3** structure.

Comparison of CNJ206 and 17E8 Active Sites. The availability of two catalytic antibody structures with esterase activity presents an opportunity to compare their active sites (Fig. 3 *Lower*). As mentioned above, the bottoms of both cavities, where the nitro group of **3** and the phenyl group of the hapten in 17E8 are located, are constituted of the same residues; they

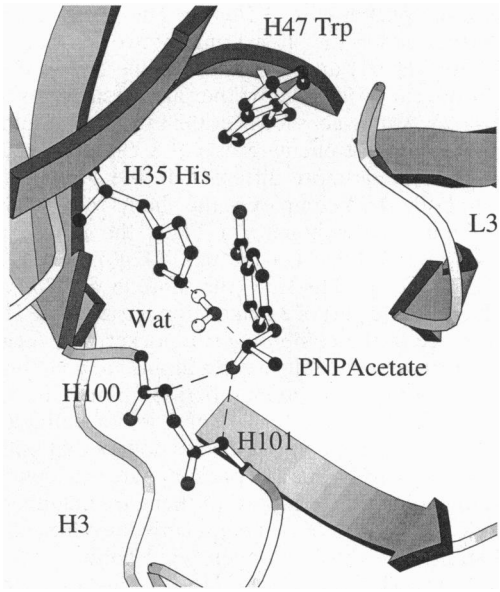

FIG. 6. Model of the general base-catalyzed mechanism for *p*-nitrophenyl ester hydrolysis by CNJ206. The *p*-nitrophenyl acetate (PNPAcetate) substrate is shown in the tetrahedral conformation of its putative transition state in the hydrolysis. The contribution of His-H35 as a general base depends on the probability that the hydrogen bond with Trp-H47 is broken; this corresponds to the configuration shown here. The attacking water is labeled Wat, and its hydrogen atoms are shown; one of them makes a hydrogen bond with unprotonated His-H35 $N^{\varepsilon 2}$. The forming bond between the Wat oxygen and the carbon of *p*-nitrophenyl acetate carbonyl is marked by a broken line. Alternatively, hydroxide attack would occur without significant base catalysis, and most of the effect of CNJ206 would be due to oxyanion stabilization.

have the same conformation. Other similarities may be discovered between the 17E8 and CNJ206 active sites as follows. (*i*) In 17E8 the oxyanion hole primarily consists of the ε-amino group of Lys-H97 (14), but comparison with the CNJ206 phosphonate stabilizing groups, involving peptide NH groups of residues H100 and H101, suggests that in 17E8, the H100 backbone NH is also involved. The distance between this group and the phosphonate oxygen located in the oxyanion hole of 17E8 is 3.2 Å, within the allowed range for a hydrogen bond. (*ii*) In 17E8 a Ser-His catalytic diad (Ser-H99/His-H35) was proposed (14) to be responsible for catalysis at the optimal pH for catalytic activity (pH = 9.5). His-H35, the base that has been proposed to activate the Ser-H99 nucleophile in the catalytic dyad of 17E8, is also present in CNJ206; when the Fv parts of both structures are superposed (rms deviation of C^{α} positions: 1.5Å; 184 atoms compared), the two His-H35 residues have very similar orientations and their C^{α} atoms deviate only by 0.6 Å. Ser-H99 of 17E8 is replaced by glycine in CNJ206; the main-chain dihedral angles of Gly-H99 are allowed for all residues. Therefore, the replacement of Gly-H99 in CNJ206 by a serine is possible without changing the conformation of the H3 loop; one of the favored rotamers of the serine residue would be positioned at a proper distance for nucleophilic attack on the substrate as was proposed to be the case in the catalytically active conformation of 17E8 (14).

Hapten Structure and the Active Site of Abzymes. Hapten design and screening methodologies are two key elements in obtaining catalytic antibodies. How do CNJ206 and 17E8 combining sites reflect the strategy followed to generate them? Phosphonates were originally chosen as haptens for hydrolytic antibodies because it was expected that they would induce combining site structures that would minimize the energetically unfavorable interactions of a tetrahedral hydrolysis transition state. The CNJ206·**3** structure and that of the complex of 17E8 with its hapten are consistent with that hypothesis: in both cases the phosphonate oxyanion is stabilized by hydrogen bond donors.

The screening methods used to select CNJ206 and 17E8 are similar. Both abzymes have been selected among the induced clones for their ability to bind a phosphonate hapten (13, 35). In both cases this criterion was satisfied in a similar way, by making hydrogen bonds to the phosphonate oxygens and by deeply burying the aromatic part of the hapten. Both structures suggest that point mutations might significantly increase catalytic activity; the corresponding clones might be present among the population of elicited antibodies, but they were not chosen from the clones secreting the tightest binding antibodies. On the basis of the available structural data, these mutants would not necessarily bind the hapten more efficiently than 17E8 or CNJ206. Therefore, to select such clones with improved activity, one would need to screen them for catalysis, as recently proposed (8, 9).

One last point deserves mention. The residues of CNJ206 and 17E8 that interact with the hapten have striking similarities (the bottom of the combining site, residue H35, and the main chain of residues H99 and H100 superpose well). However, in the superposition of the structures of the Fab·TSA complexes, the phenyl of **3** overlaps with the phosphonate hapten in 17E8; yet another difference is Lys-H97 which makes a major contribution to the oxyanion hole in 17E8 and is replaced by an alanine in CNJ206. Both antibodies bind their respective haptens in the same orientation with respect to the Fab; such a similarity arises despite the fact that these antibodies have been raised against quite different haptens, which only have O-linked aryl and phosphonate groups in common. This suggests that the bound hapten orientation observed in CNJ206 and 17E8 will often be encountered for such molecules with O-linked aryl and phosphonate groups. Variations of the residues of the combining site that affect either TSA binding (like Lys-H97 in 17E8) or catalysis (like Ser-H99 in 17E8) will depend on the precise hapten used for immunization and on the antibody selected in the screening procedure. Among the combining sites that bind the hapten in the orientation we observed here, those of CNJ206 and 17E8 might be considered as different steps towards efficient catalysts of aryl ester hydrolysis.

We are grateful to Dan S. Tawfik for providing materials and for his insightful comments on the paper. We thank O. Tchertanova and J. Janin for help and discussions. We acknowledge J. P. Benoit and R. Fourme for the use of facilities at the Laboratoire pour l'Utilisation du Rayonnement Electromagnétique (Orsay, France). This work was supported in part by a grant from the Ministère de la Recherche et de l'Enseignement Supérieur and by Contract 94/128 from Direction des Recherches Etudes et Techniques.

1. Wolfenden, R. & Radzicka, A. (1991) *Curr. Opin. Struct. Biol.* **1,** 780–787.
2. Pauling, L. (1948) *Am. Sci.* **36,** 51–58.
3. Vogtle, F. (1991) *Supramolecular Chemistry* (Wiley, Chichester, U.K.).
4. Wells, J. A., Cunningham, B. C., Graycar, T. P. & Estell, D. A. (1987) *Proc. Natl. Acad. Sci. USA* **84,** 5167–5171.
5. Evnin, L. B., Vàsquez, J. R. & Craik, C. S. (1990) *Proc. Natl. Acad. Sci. USA* **87,** 6659–6663.
6. Lerner, R. A., Benkovic, S. J. & Schultz, P. G. (1991) *Science* **252,** 659–667.
7. Huse, W. D., Sastry, J., Iverson, S. A., Kang, A. S., Alting-Mees, M., Burton, D. R., Benkovic, S. J. & Lerner, R. A. (1989) *Science* **239,** 1275–1281.
8. Tawfik, D. S., Green, B. S., Chap, R., Sela, M. & Eshhar, Z. (1993) *Proc. Natl. Acad. Sci. USA* **90,** 373–377.
9. Hilvert, D. & MacBeath, G. (1994) *J. Am. Chem. Soc.* **116,** 6101–6106.
10. Hilvert, D. (1994) *Curr. Opin. Struct. Biol.* **4,** 612–617.
11. Golinelli-Pimpaneau, B., Gigant, B., Bizebard, T., Navaza, J., Saludjian, P., Zemel, R., Tawfik, D. S., Eshhar, Z., Green, B. S. & Knossow, M. (1994) *Structure (London)* **2,** 175–183.
12. Zemel, R., Schindler, D. G., Tawfik, D. S., Eshhar, Z. & Green, B. S. (1994) *Mol. Immunol.* **31,** 127–137.
13. Tawfik, D. S., Zemel, R. R., Arad-Yellin, R., Green, B. S. & Eshhar, Z. (1990) *Biochemistry* **29,** 9916–9921.
14. Zhou, W. G., Guo, J., Huang, W., Fletterick, R. J. & Scanlan, T. S. (1994) *Science* **265,** 1059–1064.
15. Friguet, B., Djavadi-Ohaniance, L. & Goldberg, M. E. (1989) in *Immunochemical Analysis of Protein Conformation*, ed. Creighton, T. E. (IRL, Oxford), pp. 287–309.
16. Leslie, A. G. W. (1992) *CCP4 ESF-EACMB Newsletter Protein Crystallog.* **26.**
17. Collaborative Computational Project Number 4 (1994) *Acta Crystallogr. Sect. D Biol. Crystallogr.* **50,** 760–763.
18. Navaza, J. (1994) *Acta Crystallogr. Sect. A Fundam. Crystallogr.* **50,** 157–163.
19. Brünger, A. T. (1992) X-PLOR *Manual* (Yale Univ. Press, New Haven, CT), Version 3.1.
20. Brünger, A. T. (1992) *Nature (London)* **355,** 472–475.
21. Jones, T. A., Zhou, J.-Y., Cowan, S. W. & Kjeldgaard, M. (1991) *Acta. Crystallogr. Sect. A Fundam. Crystallogr.* **47,** 110–119.
22. Laskowski, R. A., McArthur, M. W., Moss, D. S. & Thornton, J. M. (1993) *J. Appl. Crystallogr.* **26,** 283–291.
23. Luzzati, V. (1952) *Acta Crystallogr.* **5,** 802–810.
24. Bernstein, F. C. & Tasumi, M. (1977) *J. Mol. Biol.* **112,** 535–542.
25. Kabsch, W. (1978) *Acta Crystallogr. Sect. A Fundam. Crystallogr.* **34,** 827–828.
26. Shrake, A. & Rupley, J. A. (1973) *J. Mol. Biol.* **79,** 351–371.
27. Wilson, I. A. & Stanfield, R. L. (1994) *Curr. Opin. Struct. Biol.* **4,** 857–867.
28. Kraulis, P. (1991) *J. Appl. Crystallogr.* **24,** 924–950.
29. Brändén, C. & Tooze, J. (1991) *Introduction to Protein Structure* (Garland, New York).
30. Jones, T. A. (1992) in *Proceedings of the CCP4 Study Weekend on Molecular Replacement*, eds. Dodson, E. J., Gover, S. & Wolf, W. (Sci. Eng. Res. Council Daresbury Lab., Warrington, U.K.), pp. 95–101.
31. Roberts, V. A., Stewart, J., Benkovic, S. J. & Getzoff, E. D. (1994) *J. Mol. Biol.* **235,** 1098–1116.
32. Fersht, A. R. (1987) *Trends Biochem. Sci.* **12,** 301–304.
33. Wells, J. A., Cunningham, B. C., Graycar, T. P. & Estell, D. A. (1986) *Philos. Trans. R. Soc. London A* **317,** 415–423.
34. Bürgi, H. B., Dünitz, J. D. & Shefter, E. (1974) *Acta Crystallogr. B* **30,** 1517.
35. Guo, J., Huang, W. & Scanlan, T. S. (1994) *J. Am. Chem. Soc.* **116,** 6062–6069.